electronic reprint

Journal of
Applied Crystallography
ISSN 0021-8898

Energy-dispersive X-ray diffraction on thin films and its application to superconducting samples

V. Rossi Albertini, B. Paci, S. Meloni, R. Caminiti and L. Bencivenni

Journal of
Applied Crystallography
ISSN 0021-8898

Received 14 February 2002
Accepted 7 October 2002

Energy-dispersive X-ray diffraction on thin films and its application to superconducting samples

V. Rossi Albertini,[a] B. Paci,[a]* S. Meloni,[b] R. Caminiti[c] and L. Bencivenni[c]

[a]Istituto di Struttura della Materia, Consiglio Nazionale delle Ricerche, Area di Ricerca di Tor Vergata, Via del Fosso del Cavaliere 100, 00133 Roma, Italy, [b]Consorzio interuniversitario per le Applicazioni di Supercalcolo per Universita' e Ricerca, Università degli Studi 'La Sapienza', Piazzale A. Moro 5, 00185 Roma, Italy, and [c]Dipartimento di Chimica, Istituto Nazionale di Fisica della Materia, Università degli Studi 'La Sapienza', Piazzale A. Moro 5, 00185 Roma, Italy. Correspondence e-mail: paci@ism.rm.cnr.it

Energy-dispersive X-ray diffraction is applied to investigate double-layer PBCO/YBCO thin films deposited by laser ablation. The merits of this technique for the structural study of films are discussed. It is shown that the rocking curves of the Bragg reflections of a film along the *c* direction can be simultaneously collected, allowing the accurate evaluation of its angular spread. A systematic displacement of the rocking curves of the film with respect to those of the substrate was found, revealing a slight divergence of the growth direction from the normal to the substrate surface.

1. Introduction

The structural study of a series of superconducting $YBa_2Cu_3O_7$ (YBCO) high-quality thin films by means of energy-dispersive X-ray diffraction (EDXD) (Manther & Parrish, 1976; Giessen & Gordon, 1968; Nishikawa & Iijima, 1984) is presented. The films were deposited by laser ablation (Venkatesan *et al.*, 1988; Beech & Boyd, 1992) on $(1\bar{1}02)$ Al_2O_3 substrate. A buffer layer of $PrBa_2Cu_3O_7$ (PBCO), having the same crystal structure as YBCO (Le Page *et al.*, 1987), was used in order to encourage the epitaxial growth of the film. At the same time, the buffer prevents contamination of the YBCO film caused by the diffusion of Al of the sapphire substrate (which affects the superconducting properties) when it is heated during the deposition (Gao *et al.*, 1992).

A crucial point to consider in the application of YBCO films in electronic device fabrication is the interrelationship between the deposition processes and the resulting microstructural properties of the deposited film. In this paper, it is shown that EDXD represents a competitive technique for elucidating such relationships. To collect a diffraction pattern by EDXD, the sample is irradiated by a continuous-spectrum X-ray beam, defined as 'polychromatic' or 'white', and the energy spectrum of the scattered radiation is acquired by an energy-sensitive detector, no movements being required. This static configuration represents the major advantage with respect to the conventional angular dispersive X-ray diffraction (ADXD) technique. The relation between the value of E at which a peak is observed and the corresponding value of the scattering parameter (q) is $q = aE\sin\theta$ ($a = 1.014$ Å^{-1} keV^{-1}), where 2θ is the scattering angle. When reflection geometry has to be used, the static setup of EDXD guarantees that the irradiated part of the sample surface is unchanged during the collection of spectra. Moreover, the whole diffraction pattern is obtained in a single measurement. The time ratio for recording an EDXD spectrum as compared to an ADXD spectrum is proportional to the ratio of the integrated photon intensity over the *bremsstralung* spectrum to the integrated intensity over the characteristic $K\alpha$ line. Depending on the target material and the settings for the high voltage and the current, the time saving for recording an EDXD spectrum can be appreciable. For our experimental conditions this factor was about 10 and an equivalent reduction of the acquisition time of the rocking curves was obtained. This is particularly important when thin films are analysed, since the scarcity of the material available for the scattering may make the measurement of diffraction patterns with acceptable signal to noise ratios difficult and time consuming.

2. Experimental

2.1. Samples

The samples studied were YBCO epitaxial thin films grown on PBCO buffer layers deposited on a sapphire single-crystal substrate. The YBCO/PBCO system was produced using pulsed excimer laser ablation (Giardini Guidoni *et al.*, 1997; Chang Hoi Hur & Sang Yeol Lee, 2001) from stoichiometric high-density ceramic targets (Giardini Guidoni *et al.*, 1994). A 308 nm XeCl excimer laser was focused onto the target with an energy density of about 3 J cm^{-2}, using identical growth conditions for both layers, at a temperature of 993 K and under an oxygen pressure of 30 Pa, with typical growth rates of 2 Å s^{-1}. The thermal regulation was performed by a CO_2 laser heating source, controlled by a substrate-holder thermocouple. After deposition, the samples were cooled to 723 K at 10 K min^{-1}. The experimental setup has been described in full by Romeo *et al.* (1991). In all the samples, the YBCO film

Table 1
α_0 and full width at half-maximum (FWHM) values for each sample.

Sample	α_0 (°)	FWHM (°)
PBCO 200 Å/YBCO 500 Å	0.326 (6)	0.797 (17)
PBCO 400 Å/YBCO 500 Å	0.108 (21)	0.975 (70)
PBCO 600 Å/YBCO 500 Å	0.188 (16)	1.032 (45)
PBCO 800 Å/YBCO 500 Å	0.118 (13)	0.975 (38)
PBCO 1000 Å/YBCO 500 Å	0.189 (24)	1.000 (80)

had a thickness of 500 Å, while the PBCO buffer-layer thickness was variable (200, 400, 600, 800 and 1000 Å).

2.2. The diffractometer

The energy-dispersive diffractometer, shown in Fig. 1, is a non-commercial instrument equipped with a water-cooled X-ray W anode tube (Philips, model PW2214/20) operating at 58 kV and 30 mA. The white beam is collimated by two W slits and reaches the sample placed in the centre of rotation of the diffractometer arms. The two slits of the second arm select the portion of the diffracted beam contained in the acceptance angle of the detecting system, which is an EG&G ultra-pure Ge solid-state detector (SSD), cooled by a liquid-nitrogen bath and connected to an integrated spectroscopy amplifier–multichannel analyser system (92× Spectrum Master).

2.3. The experimental method

The rocking curves of the Bragg reflections of the film were measured as a function of the asymmetry parameter $\alpha = (\theta_i - \theta_r)/2$, where the incidence angle θ_i and the reflection angle θ_r are defined with respect to the sample surface (see Fig. 2). The distribution of the diffracted intensity as a function of α, keeping $\theta_i + \theta_r = 2\theta$ unchanged, reproduces the statistical distribution of the domain orientation.

The purpose of the present work was to measure all the rocking curves of the film's Bragg reflections simultaneously.

The adopted experimental procedure is as follows. The sample is positioned on a cradle, as shown in Fig. 2, placed in the centre of the diffractometer. According to the definition of the scattering parameter, the amplitude of the q interval scanned in a single measurement is proportional to $\sin\theta$. Therefore, the setting of the diffractometer arms must correspond to an angle that is sufficiently high to see several peaks. Then, keeping the inclination of the arms fixed, the cradle is progressively rotated until the maximum diffracted intensity is reached.

This maximum intensity is due to the substrate reflections, since the ratio between the film thickness and the substrate thickness is several orders of magnitude. Therefore, this is the symmetry condition $\alpha = 0°$ for the substrate, which we assumed as the reference position.

Since the film tends to grow with the c axis approximately perpendicular to the substrate lattice planes, the film reflections must have maximum intensity not far from this reference position.

At constant 2θ, an α scan is performed by carrying out a sequence of diffraction measurements. Starting from a value at which the diffracted intensity is very low ($\alpha = -2°$), α is progressively increased in steps of 0.1°, until the opposite position is reached ($\alpha = 2°$). The definition of q implies that its value is constant when 2θ is fixed. Nevertheless, the components of q along ($q_{\|}$) and perpendicular to ($q_{\perp}$) the normal to the film surface depend on α (see the inset of Fig. 2). However, at small α values, the variation of $q_{\|}$ is negligible, since $q_{\|} = q\cos\alpha$, while $q_{\perp} = q\sin\alpha$ increases linearly with α. Therefore, at different α ($q_{\perp}$), the intensities of the peaks change, but their positions do not. After the diffraction data are processed

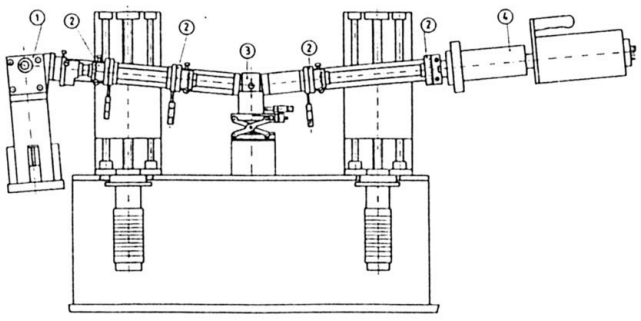

Figure 1
Sketch of the energy dispersive X-ray diffractometer. The fundamental components are: (1) X-ray source (W anode tube), (2) collimation slits, (3) sample holder, (4) Ge single-crystal energy-sensitive detector.

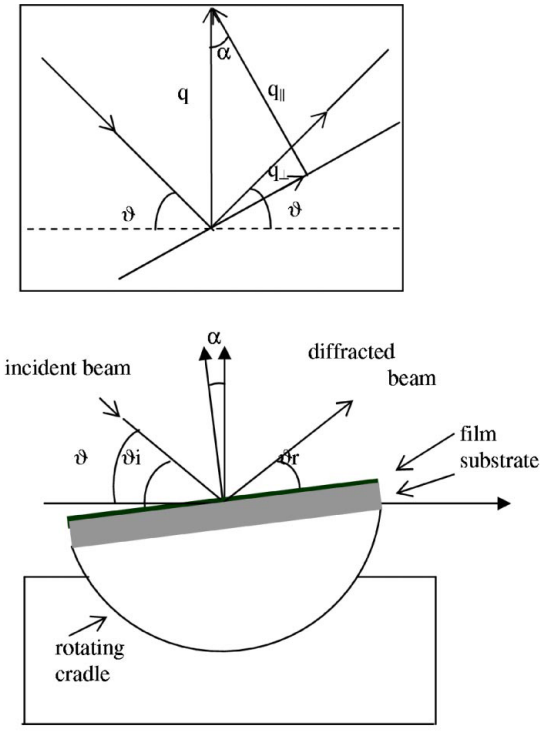

Figure 2
Scheme of the geometric setup. The films are positioned on a cradle placed at the centre of rotation of the diffractometer. The measurements are performed by rotating the cradle, *i.e.* for different values of the asymmetry parameter $\alpha = (\theta_i - \theta_r)/2$, keeping the diffraction angle 2θ unchanged. For clarity, the angle of rotation of the cradle is emphasized ($\alpha = 7°$), as well as the film thickness.

(see below), the curves of the peak intensities can be plotted as a function of α. Since in EDXD the peaks are measured simultaneously, an equivalent number of rocking curves is obtained and statistical information can be obtained: the mean value of the angular distribution of the c axis of the grains and the standard deviation from it.

In our case, the substrate lattice structure is much more ordered than that of the film. Consequently, the Bragg reflections of the substrate are visible at low $|\alpha|$ values only, while the film reflections are still present when the substrate no longer reflects ($\alpha \simeq 1$–2°). For this reason, rotating the cradle sufficiently, only the film diffraction peaks are visible, despite the film being 10^4–10^5 times thinner than the substrate, so that the film can be observed under conditions in which only Compton and the thermal diffuse scattering cause effects.

3. Results and discussion

Each rocking curve is calculated as the ratio between the intensity of a Bragg peak corresponding to a generic α with respect to the maximum intensity of the same peak along the α scan. Therefore, unlike the standard EDXD measurements that require complex data processing, in the present case the rocking-curve calculation is quite easy. In fact, all the phenomena that contribute to the modification of the diffraction pattern (energy spectrum of the primary beam, X-ray absorption, Compton scattering) are independent of α and can be either neglected or removed in the following way. The normalization to the primary beam intensity, which is necessary in measurements of lattice parameters since every diffraction peak is proportional to the energy component of the primary beam producing it (Caminiti & Rossi Albertini, 1999), is not required in our case. Indeed, the experimental points of each rocking curve are calculated as the ratio between the intensities of a single Bragg reflection, which is produced by the same energy component of the primary white beam, at two different α values. The absorption is negligible, being proportional to the exponential of the film thickness, while Compton scattering is taken in account during the fitting of the diffraction peaks.

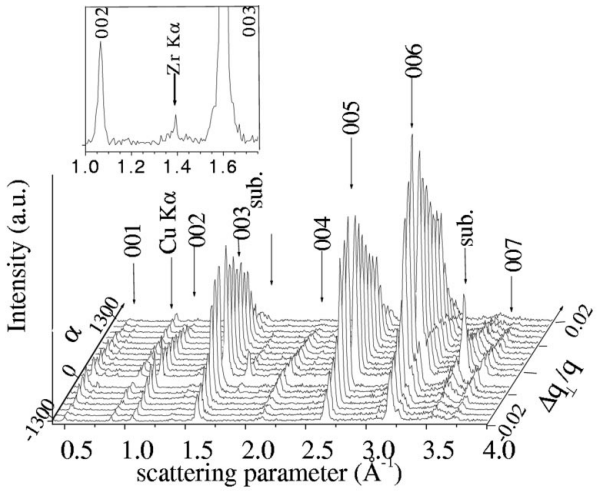

Figure 3
Sequence of the EDXD patterns for the PBCO 400 Å/YBCO 500 Å sample acquired during the α scan. The film reflections are indexed. The inset reports only one of the recorded spectra, in a narrower q range: the fluorescence line of Zr is at 1.40 Å^{-1}, which, at this angle, corresponds to 15.75 keV.

The corrected data are fitted using the sum of a Gaussian function and a linear one: the Gaussian component reproduces the convolution of the Bragg peak with the diffractometer resolution function, while the linear function reproduces the almost flat background and the smooth Compton profile. The Gaussian integral is proportional to the coherent scattered intensity, used to calculate the rocking curve, while its maximum indicates the position of the Bragg peak, required to obtain the interplanar distance along the c axis.

Since X-ray diffraction provides information about the lattice structure in the direction of the scattering vector, a measurement of the rocking curves of the film perpendicular to the c direction allows the evaluation of both its degree of epitaxiality and a possible misalignment of the average orientation of its domains with respect to the average orientation of the substrate domains. Actually, the orientation of the c axis of the crystalline domains exhibits a sharp distribution around its average value, while the a and b axes are oriented randomly (Boffa *et al.*, 1993). The relation $d(00n) = 2\pi n/q(00n)$ is used to calculate the interplanar spacing along the c axis, where $d(00n)$ is the distance between planes calculated on the basis of the $(00n)$ reflections. The average value of the parameter is 11.66 (12) Å, in good agreement with the literature data.

In Fig. 3, we show the normalized diffraction patterns of the PBCO 400 Å/YBCO 500 Å sample collected at various α, keeping the total scattering angle ($2\theta = 12.58^\circ$) unchanged. Several diffraction peaks are visible, the major ones of which are at 1.601, 2.668 and 3.203 Å, which can be assigned to the 003, 005 and 006 reflections used for the rocking-curve computation. The gap in the α scan plot at $\alpha = 0^\circ$ is due to the fact that the spectrum corresponding to the maximum intensity of the substrate is omitted because the substrate reflections are too strong and compromise the visibility of the film reflections.

One of the qualities of the EDXD technique is the possibility of gaining diffractometric and spectroscopic data simultaneously. This characteristic allows the detection of the presence of possible chemical impurities in the film. Indeed, in Fig. 3, besides the fluorescence lines produced by the chemical species belonging to the film and to the substrate, another line corresponding to the fluorescence of Zr can be noticed. Actually, this element is a constituent of the crucible in which the YBCO and PBCO tablets, used as the targets of the laser beam during the ablation, are melted. At the high temperature required for melting, Zr diffuses in the target material, contaminating it slightly.

Observing Fig. 3, it can be noticed that increasing the α value, the substrate reflection intensity rapidly decreases, while the film reflection intensity decreases much slower, as expected for the higher crystalline quality of the sapphire

substrate with respect to the poorer texture of the laser-ablated film.

The fit of each peak having a structure factor sufficient to give an appreciable scattered intensity was accomplished. The results show that the epitaxiality index, estimated as the mean value of FWHM of the fit [equal to $2(2\log 2)^{1/2}\sigma$], is about 0.9 (2)°. The fluctuations around the mean value seem not to depend on the PBCO buffer layer thickness. This indicates that, if a correlation occurs between this thickness and the mosaic spread of YBCO, it would produce effects on the epitaxiality of less than 0.2°.

Finally, the rocking curves for the PBCO 200 Å/YBCO 500 Å, PBCO 400 Å/YBCO 500 Å, PBCO 600 Å/YBCO 500 Å, PBCO 800 Å/YBCO 500 Å, and PBCO 1000 Å/YBCO 500 Å samples, calculated as discussed above, are shown in Fig. 4. The maximum of each rocking curve does not coincide with the reference value ($\alpha = 0°$) at which the intensity of the substrate reflections is the highest, but is displaced systematically by about 0.33, 0.11, 0.19, 0.12, and 0.19°, respectively (see Table 1). This can be attributed to the effect of the miscut of the substrate on the film orientation.

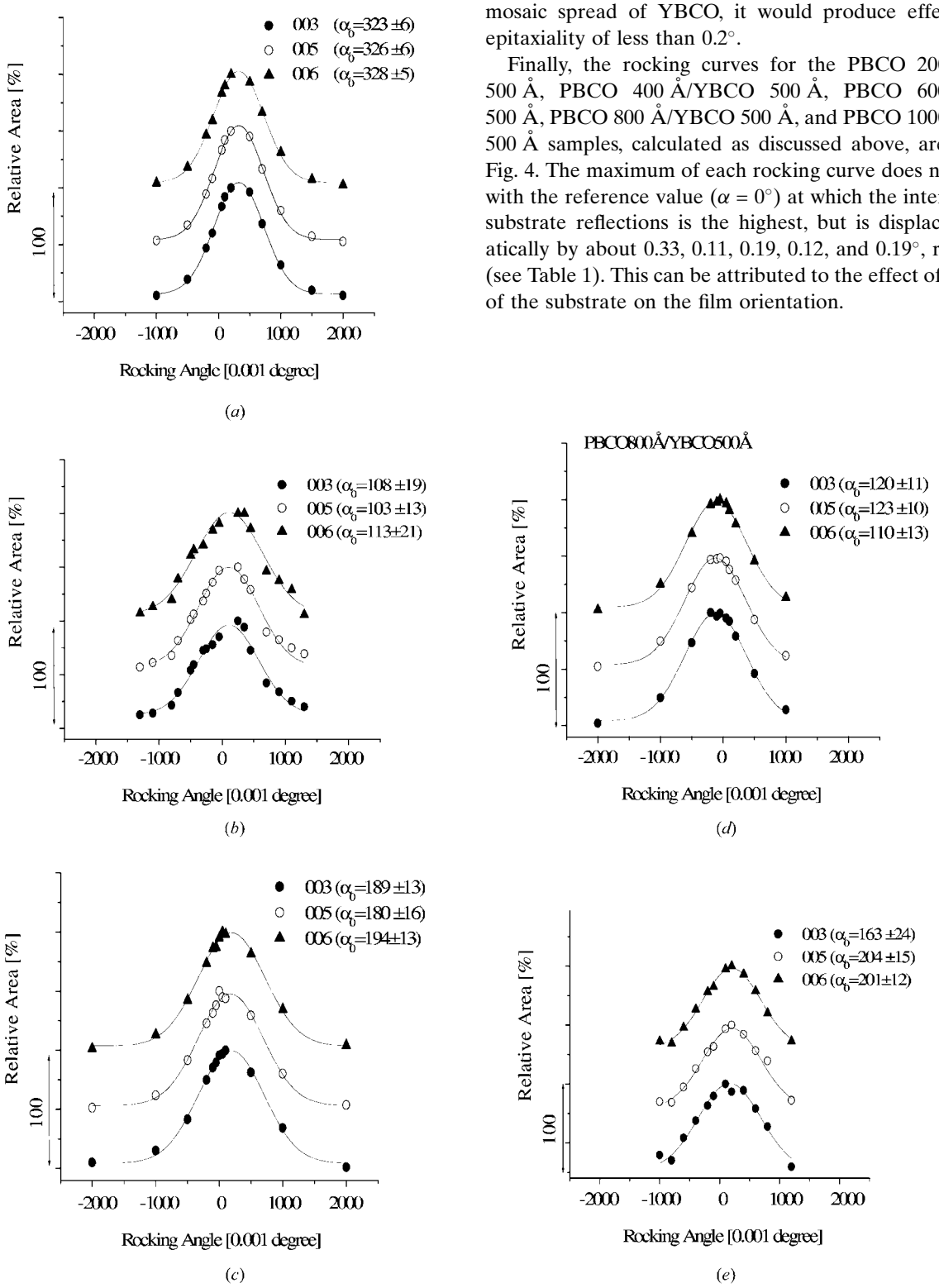

Figure 4
Rocking curves of (*a*) PBCO 200 Å/YBCO 500 Å, (*b*) PBCO 400 Å/YBCO 500 Å, (*c*) PBCO 600 Å/YBCO 500 Å, (*d*) PBCO 800 Å/YBCO 500 Å, (*e*) PBCO 1000 Å/YBCO 500 Å. For each sample the rocking curves relative to the 003, 005 and 006 peaks are reported (shifted for clarity). The central value of the rocking angle α_0 is reported in the legend (units of 0.001°).

4. Conclusions

We have presented the results of an EDXD-based method to measure YBCO superconducting thin films. The technique is shown to be very useful for this purpose, giving a straightforward method for the determination of all the Bragg reflection rocking curves. The five samples we investigated differ in the thickness of the buffer layer of PBCO, used to prevent contamination of the YBCO film by the sapphire substrate during the deposition process by laser ablation. The results show that for each sample the rocking curves of the different reflections coincide, within experimental uncertainty. Comparing the results obtained for different samples, we observe that the thickness of the buffer layer does not modify the film structure; in fact, the rocking-curve FWHM does not depend on the film thickness.

References

Beech, F. & Boyd, I. W. (1992). *Photochemical Processing of Electron Materials*, pp. 387–388. New York: Academic Press.

Boffa, V., Paternò, G., Romeo, C., Rossi, V., Penna, M., Di Gioacchino, D., Gambardella, U., Barbanera, S. & Murtas, F. (1993). *IEEE Trans. Appl. Supercond. '93*, pp. 1068–1072.

Caminiti, R. & Rossi Albertini, V. (1999). *Int. Rev. Phys. Chem.* **18**, 263–299.

Chang Hoi Hur & Sang Yeol Lee (2001). *Thin Solid Films*, **398**, 444–447.

Gao, J., Klopman, B. B. G., Aarnink, W. A. M., Reitsma, A. E. & Gerritsma, G. J. (1992). *J. Appl. Phys.* **71**, 2333–2337.

Giardini Guidoni, A., Ferro, D., Gambardella, U., Marotta, V., Martino, R., Morone, A. & Orlando, S. (1994). *Thin Solid Films*, **241**, 114–118.

Giardini Guidoni, A., Mele, A., Di Palma, T. M., Flamini, C., Orlando, S. & Teghil, R. (1997). *Thin Solid Films*, **295**, 77–82.

Giessen, B. C. & Gordon, G. E. (1968). *Science*, **159**, 973–974.

Le Page, Y., Siegrist, T., Sunshine, S. A., Seemeyer, L. F., Murphy, D. W., Zahurak, S. M., Waszczak, J. V., McKinnon, W. R., Tarascon, J. M., Hull, G. W. & Greene, L. H. (1987). *Phys. Rev. B*, **30**, 3617–3621.

Manther, M. & Parrish, W. (1976). *Energy Dispersive X-ray Diffractometry*, in *Advances in X-ray Analysis*, Vol. 20, pp. 1–186. New York: Plenum.

Nishikawa, K. & Iijima, T. (1984). *Bull. Chem. Soc. Jpn*, **57**, 1750–1759.

Romeo, C., Boffa, V., Bollati, S., Paternò, G., Alvani, C., Penna, M., Barbanera, S., Castrucci, P., Leoni, R. & Murtas, F. (1991). *Physica C*, **180**, 77–80.

Venkatesan, T., Wu, X. D., Inam, A. & Wachtma, J. B. (1988). *Appl. Phys Lett.* **27**, 2293–2298.